

¹ Characterizing water level responses to barometric pressure fluctuations
² from seconds to days

³ Jonathan Kennel^a, Beth Parker^a

^aUniversity of Guelph School of Engineering 50 Stone Road East Guelph Ontario N1G 2W1 Canada

⁴ **Abstract**

A regression deconvolution method using distributed lags for the efficient calculation of barometric/loading response functions in the presence of Earth tides and background trends was applied to water pressure measurements collected every second. This method was able to simultaneously deconvolve multiple stresses that can be used for both signal decomposition (removal of noise and isolation of signals) and the determination of impulse response functions that can be interpreted for hydraulic properties and subsurface characterization. We also demonstrate how the static barometric efficiency is a deficient parameter when applied to wells having delayed responses and needs to be applied with care. The distributed lag method combined with high frequency monitoring has implications for improved site characterization, determining the continuity of subsurface features, parameter estimation, understanding the degree of confinement, and signal decomposition. The methods for this paper can be found in the R *hydrorecipes* package.

*Corresponding author

Email addresses: jkennel@uoguelph.ca (Jonathan Kennel), bparker@uoguelph.ca (Beth Parker)

5 **Introduction**

6 Water levels are constantly changing due a variety of stresses such as barometric pressure, Earth and
7 ocean tides, surface water levels, precipitation, pumping and injection, loading and unloading, earthquakes
8 to name a few. Not only do they respond to nearby stress changes but they can respond to changes
9 originating thousands of miles away, which travel through different volumes of the subsurface. These water
10 level fluctuations may be small (sub-millimeter) or large (meters) and be short (sub-second) or long-lived
11 (days to years). Historical and present technical limitations lead to many of these changes going unnoticed or
12 unrecognized due to inadequate monitoring frequency and insufficient equipment precision. As monitoring
13 technology continues to improve, new analysis methods will be necessary to better interpret the multitude
14 of water level responses. To evaluate what can be gained by using higher frequency measurements, water
15 pressures were collected every second for multiple months at a fractured sandstone site. Using natural stress
16 changes caused by barometric pressure, ambient water pressure responses are probed at a temporal scale not
17 commonly examined. The barometric response is important for three primary reasons: barometric responses
18 are present in water levels across the Earth (data is widely available); the response is related to subsurface
19 parameters and character (information rich, i.e. hydrogeologic insights); and the removal of the barometric
20 response can reveal previously obscured signals (improved data quality via noise reduction).

21 In this paper we define high frequency as a sampling interval that is less than one minute, which contrasts
22 with common sampling intervals for ambient monitoring of 5 minutes or greater. The collection of high
23 frequency data for long periods of time (months to years) requires equipment with suitable memory and power
24 so that they can operate for months at a time with minimal intervention. In addition, a clear motivation
25 for collecting the high frequency data is necessary and we hope this paper encourages the collection of higher
26 frequency data to improve subsurface characterization and parameterization. Historically the technological
27 limitations and associated costs likely contributed to lower data collection frequencies, however, many of
28 the technical limitations are being addressed with inexpensive memory and low power consumption devices.
29 In addition, following data collection, new methods may be required to be able to evaluate the larger
30 data sets. The goal of this paper is to introduce a time domain method that can be used to characterize
31 water level responses and encourage others to collect high frequency data to advance decision-making and
32 scientific understanding. First, methods are applied to a synthetic example with known properties, followed
33 by examples with field data from a sandstone site. While this paper focuses on the barometric response, the
34 methods can also be applied to other responses such as river stage, pumping, precipitation and others.

35 The relationship between water levels (or water pressures) and barometric pressure is often conceptualized

36 with a single value - the barometric efficiency (Jacob, 1940; Clark, 1967; Davis and Rasmussen, 1993;
37 Gonthier, 2007; Smith et al., 2013; Acworth et al., 2016; Turnadge et al., 2019). This relationship assumes
38 a confined aquifer with an instantaneous response to changes in barometric loading. While many methods
39 exist to estimate barometric efficiency, there is a key deficiency of single value (BE) methods that goes
40 beyond their ability to handle noise (non-barometrically induced changes) in the data set; they assume a
41 lag free or frequency independent response. To have an instantaneous response, the formation must respond
42 (deform) instantly and the monitoring well must represent the formation pressure without any time lag. In
43 practice, there is often a finite amount of time required for a signal to propagate through the subsurface and
44 generate changes at the monitoring well (Hvorslev, 1951). These changes may occur rapidly (seconds) or
45 slowly (days) depending on the source of the stress, the well design and geologic properties. Characterizing
46 delayed or lagged responses can be difficult due to equipment limitations, the signal to noise ratio, interfering
47 signals, and inadequate monitoring where the monitoring frequency is too low or the associated input signals
48 (barometric pressure, precipitation, etc.) are collected too far away from the monitoring well.

49 The limitation of using a single barometric efficiency can be overcome by describing the barometric
50 response with a time lag or frequency dependence. Barometric response functions were introduced to
51 solve this problem and expand the notion of barometric efficiency to semi-confined and unconfined systems
52 (Rojstaczer, 1988; Rasmussen and Crawford, 1997; Toll and Rasmussen, 2007; Rasmussen and Mote, 2007;
53 Odling et al., 2015). These methods provide additional information over the traditional barometric efficiency
54 that can provide diagnostic information about the subsurface. For example, Rojstaczer (1988) describes four
55 imbalances that occur after a barometric pressure change for a semi-confined aquifer: (1) Vertical air flow
56 in the vadose zone to the water table (vadose response); (2) vertical groundwater flow between the water
57 table and the confining layer; (3) vertical groundwater flow between the aquifer and confining layer; and (4)
58 Lateral groundwater flow between the formation and well (well-bore storage). While the pressure imbalances
59 are established instantly, the lagged (or frequency dependent) response propagates through different volumes
60 of the subsurface and occurs over multiple time scales. A single value is unable to describe these changes and
61 the timing and magnitude of the response is related to subsurface and well properties. The first (1) imbalance
62 will be related to the thickness and pneumatic diffusivity of the vadose zone (Weeks, 1979; Furbish, 1991;
63 Rojstaczer, 1988; Kuang et al., 2013; Yang and Shibata, 2020), imbalances (2) and (3) are influenced by the
64 vertical hydraulic diffusivity of the aquifer(s) and confining layer (Butler et al., 2011; Rojstaczer, 1988; Ritzi
65 et al., 1991), and imbalance (4) is related to the well geometry and formation transmissivity (Hvorslev, 1951;
66 Rojstaczer, 1988) (Figure 1). In theory, the parameters associated with these responses should be obtainable

67 by fitting the appropriate model to the barometric response function, but in practice this continues to be
68 a difficult task. Hussein et al. (2013) presented a series of theoretical barometric response functions in the
69 frequency domain to demonstrate the sensitivity of the barometric response to different aquifer, confining
70 layer, and vadose zone properties. These values are calculated for multiple scenarios and the responses
71 vary over eight orders of magnitude in the frequency domain (10,000 to 0.0001 cycles per day), however, the
72 typical empirically determined barometric response in the literature covers less than two orders of magnitude
73 (15 minutes to one day time lag or 0.02 to 2 cycles per day). Lai et al. (2013) presented coherent barometric
74 responses up to 30 cycles per day and this frequency remains uncommon. Researchers have long known about
75 the importance of frequency dependent responses but four primary reasons for the lack of field examples
76 are: (1) technical limitations of monitoring devices (2) water levels are rarely collected at high frequency;
77 (3) the increased computational effort required for larger data sets; and (4) increased cost of monitoring.

78 This paper introduces the R *hydrorecipes* package, which provides methods to better understand hy-
79 draulic responses (Kennel and Parker, 2022). R is a programming language with statistical roots and a
80 growing user community (R Core Team, 2024). The *hydrorecipes* package was heavily influenced by the
81 *recipes* package, a popular framework for pre-processing and feature engineering (Kuhn and Wickham,
82 2022). The goal of the package is to provide tools that can be efficiently applied to moderately large data
83 sets (millions of observations). For this study, the monitoring frequency for barometric and water pressure
84 was selected to be every second to characterize a larger portion of the barometric response than previously
85 explored. The *hydrorecipes* package handles increasing computational demands by modifying the lagging
86 method of Rasmussen and Crawford (1997) to use distributed lag models that can efficiently scale to much
87 larger data sets. Distributed lag models are common in econometrics and are ideally suited to smoothly
88 varying responses (Almon, 1965; Haugh and Box, 1977; Gasparrini, 2011). The method is first tested on a
89 synthetic data set and then applied to high frequency data collected every second from conventional mon-
90 itoring wells at a mountainous, semi-arid, fractured sandstone site. With the higher frequency data, the
91 ability to estimate subsurface properties is improved by increasing the ability to fit models to a larger range
92 of time lags or frequencies and thus evaluate rapid responses that correspond to higher diffusivity systems.

93 **Background and Methods**

94 *Barometric efficiency*

95 Water level changes due to barometric pressure fluctuations are commonly described by a single value,
96 the barometric (or loading) efficiency (Jacob, 1940; Clark, 1967; Gonthier, 2007; Smith et al., 2013; Acworth
97 et al., 2016; Hendry et al., 2018; Rau et al., 2020). Single value methods work best on confined systems with
98 minimal well-bore storage; however, in practice they are often applied to more complicated scenarios having
99 lagged or frequency dependent responses. The barometric/loading efficiency can be estimated in multiple
100 ways and is being used for the estimation of specific storage, therefore, representative and accurate values
101 are necessary (Turnadge et al., 2019; McMillan et al., 2020; Rau et al., 2022). A goal of many of these
102 methods is to isolate the water level changes that result solely from barometric pressure changes. This may
103 involve the inclusion of secondary variables like Earth tides or trend removal using first differences. The
104 barometric efficiency (BE) relates a portion of a barometric pressure change to a water level change and can
105 be described with the following equation:

$$BE = -\frac{\Delta WL}{\Delta P_{baro}} \quad (1)$$

106 where ΔWL is the change in water level, and ΔP_{baro} is a change in barometric pressure. The related
107 property called the loading efficiency (LE) is defined as the change in absolute pressure as a fraction of the
108 barometric pressure change and is related to the barometric efficiency by the equation:

$$LE = 1 - BE \quad (2)$$

109 For confined aquifers the barometric efficiency can also be related to the specific storage (S_s) modified from
110 Jacob (1940) equation 43:

$$S_s = \frac{\rho_w g \theta_E C_w}{BE} \quad (3)$$

111 where S_s is the specific storage, ρ_w is the density of water, θ_E is the effective porosity of the formation, and
112 C_w is the compressibility of water. The density of water and the compressibility of water are often assumed,
113 leaving the effective porosity and barometric efficiency to be estimated.

114 *Barometric Response Functions*

115 While these definitions may work for the ideal confined well with minimal well-bore storage, many wells
116 in complex geologic environments do not behave in an ideal manner. In these cases, a single value is limited,
117 does not provide the context necessary for interpretation, and can be misleading. To interpret results a more
118 complete analysis of the time or frequency dependent response is necessary. One method to examine the time
119 dependent response was introduced by Munk and Cartwright (1966) and was later applied to barometric
120 pressure responses in groundwater (Weeks, 1979; Furbish, 1991; Rasmussen and Crawford, 1997; Spane,
121 2002; Butler et al., 2011). This method calculates an impulse response using regression deconvolution and
122 has been implemented in the freely available BETCO, KGS programs, and the <https://groundwater.app>
123 which use equally spaced (regular) lags (Toll and Rasmussen, 2007; Bohling et al., 2011). The equation for
124 regularly spaced lags from Rasmussen and Crawford (1997) can be written as:

$$P_{wl-b}(t) = \sum_{i=0}^n \beta_i P_b(t - i) \quad (4)$$

125 where P_{wl-b} is the component of water pressure due to barometric pressure, P_b is the barometric pressure,
126 n is the maximum lag of the model, i is the time lag, and t is the time and β_i are the regression coefficients
127 to be determined. To minimize the effect of background trends and noise in the data, this formula is often
128 written in terms of first differences:

$$\Delta P_{wl-b}(t) = \sum_{i=0}^n \beta_i \Delta P_b(t - i) \quad (5)$$

129 where ΔP_{wl-b} is the change in water pressure due to barometric pressure, ΔP_b is the change in barometric
130 pressure occurring over some time period, typically the monitoring frequency but it could also be an integer
131 multiple of the monitoring frequency.

132 While these methods work well with data sets with tens to hundreds of lag terms (β_i) and thousands
133 of observations, they can suffer from multicollinearity and become computationally inefficient for thousands
134 of lags and millions of observations which is the case for high frequency data. Multicollinearity arises when
135 regressors are highly correlated and lagged regressors will likely be correlated particularly when sampling
136 frequency is high. In many instances the the effect of multicollinearity can be safely ignored, but it results
137 in elevated standard errors for the coefficients. Two alternative methods for doing regression deconvolution
138 that can scale to larger data sets and minimize multicollinearity are proposed. The first method uses the
139 non-difference version of the regression deconvolution equation but determines β_i at irregularly spaced lags:

$$P_{wl-b}(t) = \sum_{k=1}^m \beta_{i(k)} P_b(t - i(k)) \quad (6)$$

140 where m is number of lagged terms in the model, and k is the lag term number. The implementation of
 141 the method should have many lag terms where the response is expected to change most rapidly (typically
 142 early lag times) and fewer lag terms when the response is slowly varying (late lag times) and in practice
 143 logarithmically spaced lags are often suitable. In some ways this could be thought of as a manual form of lasso
 144 regression (L2 penalty) where terms that do not provide much additional information are manually zeroed
 145 out (excluded from the model) (Tibshirani, 1996). The number of regressors can often be decreased from
 146 many thousands to hundreds but the model may still suffer from multicollinearity and not be applicable to
 147 data sets with millions of observations. Distributed lag models provide additional efficiency for these larger
 148 data sets (Almon, 1965; Haugh and Box, 1977; Gasparini, 2011):

$$P_{wl-b} = \sum_{j=1}^m \beta_j s_j(x) \quad (7)$$

149 where j is the basis function index, s_j is the j^{th} basis variable determined by convolving P_b and the j^{th}
 150 basis function. The basis functions can be determined in a variety of ways but B-splines are popular, quick
 151 to generate, piecewise continuous, and the derivatives are commonly continuous and therefore suitable for
 152 modeling a variety of responses (Wang and Yan, 2021, 2024). The convolution can be done in the time or
 153 frequency domain and for regularly spaced data the frequency domain convolution will typically be more
 154 computationally efficient. To further elaborate on this method, suppose we want to model 30 days of data
 155 collected every second ($n = 86400 * 30 = 2592000$ measurements) with up to 4 days of lags ($m = 86400$
 156 $* 4 + 1 = 345601$ lags). The standard approach would require a regressor term for each one of these lags
 157 and the generated matrix would end up being ($n \times m = 2592000 \times 345601$). The distributed lag method
 158 aims to reduce this and starts by selecting a basis function generator (e.g. B-splines) and the number or
 159 locations of knots (e.g. at 0, 1, 10, 100, 1000, 10000, 100000, 345600 lag time and $j = 8$ for this set), which
 160 are the points where the piecewise polynomial functions meet and curvature can vary. By spacing knots
 161 closer together at early lag times, we attempt to better capture the response where it is changing most
 162 rapidly. An m (number of lags) $\times j$ (number of basis functions) matrix is then created by specifying the
 163 lag vector (0 to 345600), the knots, and other arguments to the B-spline generator (e.g. intercept, degree).
 164 Each column of this matrix is then convolved with the 30 days of barometric pressure data and results in
 165 an $n \times j$ (2592000×8) matrix of regressors. So instead of having a 2592000×345601 matrix, we end up

166 with a 2592000 x 8 matrix. This technique decreases the number of regressors (or columns of the regression
 167 matrix) by assuming the barometric response function is smoothly variable in time so a set of curves can
 168 describe the response. Knots define regions of the response where polynomial parameters in the regression
 169 vary (i.e. changes in response curvature). For barometric response functions we suggest logarithmic spacing
 170 for the lags and knots in the irregular spaced and distributed lag models respectively. Distributed lag models
 171 further decrease the required number of regressors and are less influenced by multicollinearity.

172 *Building and fitting the regression deconvolution model*

173 In the section above we describe how the regression terms are created for the different lagging methods.
 174 While barometric pressure responses are commonly found in water pressure or water level data sets, they
 175 are not the only stressor of importance. Therefore, the regression model needs to include multiple stresses
 176 and terms in addition to the barometric response. To do this, a matrix of regressors is generated which is
 177 based on the data sets that contribute to water pressure responses. For example, this may include Earth
 178 tides, pumping, precipitation, ocean levels, or other signals. In some cases the appropriate auxiliary data
 179 is absent and a regression spline can be helpful to capture background trends not related to barometric
 180 pressure or the desired signals to analyze. For example if we have a water pressure dataset that contains a
 181 barometric response and a background trend the regression equation in matrix form could be written as:

$$\begin{bmatrix} P_1^{wl} \\ P_2^{wl} \\ \vdots \\ P_n^{wl} \end{bmatrix}_{n \times 1} = \begin{bmatrix} s_1^1 & s_1^2 & \dots & s_1^j & t_1^1 & t_1^2 & \dots & t_1^k \\ s_2^1 & s_2^2 & \dots & s_2^j & t_2^1 & t_2^2 & \dots & t_2^k \\ \vdots & \vdots & \vdots & \vdots & \vdots & \vdots & \ddots & \vdots \\ s_n^1 & s_n^2 & \dots & s_n^j & t_n^1 & t_n^2 & \dots & t_n^k \end{bmatrix}_{n \times m} \begin{bmatrix} \beta_{s^1} \\ \beta_{s^2} \\ \vdots \\ \beta_{s^j} \\ \beta_{t^1} \\ \beta_{t^2} \\ \vdots \\ \beta_{t^k} \end{bmatrix}_{m \times 1} \quad (8)$$

182 where $P_{1:n}^{wl}$ are the water pressure observations, $s_{1:n}^{1:j}$ are the distributed lag terms for barometric pressure,
 183 $t_{1:n}^{1:k}$ are the regression spline terms for the background trend, and $\beta_{s^{1:j}}$ and $\beta_{t^{1:k}}$ are the coefficients to be
 184 determined by the regression for the barometric pressure and background trend respectively. Additional
 185 regressors, such as Earth tides can be added to the model in similar manner and allow all coefficients to be
 186 solved simultaneously.

187 In this format, the equation can be solved in a number of ways, with least squares regression being
188 one of the most common. However, as in the case with the traditional regularly spaced lagged models of
189 Rasmussen and Mote (2007), it is also possible to use generalized linear models with different regularization
190 constraints that can reduce the problems of overfitting. Once the regression equation is solved and the
191 coefficients determined, these coefficients can be multiplied by the regressor columns to determine the
192 contribution for each regressor group (i.e. barometric pressure and background trend components) or used
193 for prediction. Similar to regression with regularly spaced lags, the standard error of the coefficients and
194 coefficient confidence intervals can be determined and used to evaluate the precision of each individual
195 coefficient in the model and whether each coefficient is statistically significant.

196 *Synthetic responses*

197 Determining the barometric response from field data is error prone due to the presence of confounding
198 signals, non-linearities, violation of model assumptions, noise, and error in collected data sets. Many studies
199 have estimated barometric responses using field data where the true solution is unknown; however, method
200 comparison using synthetic data with a known solution can provide increased clarity.

201 Synthetic water pressures were generated by convolving loading response kernels (i.e. the response as a
202 function of time or frequency) with field measured barometric pressure data (Figure 2). Four scenarios were
203 tested: (1) Confined response; (2) Vadose response; (3) Well-bore storage response; and (4) a combined
204 vadose and well-bore storage model. The confined response kernel is a single loading value equal to 0.38
205 and leads to a water level that is a scaling of the barometric pressure. The vadose kernel used in the vadose
206 response was calculated using the 1-D air flow model of Weeks (1979) considering a unit change in barometric
207 pressure calculated for multiple times:

$$\Delta P_{wl}(t) = 1 - \frac{4}{\pi} \sum_{m=1,3,5,\dots}^{\infty} \left[(-1)^{(m-1)/2} \frac{1}{m} \exp(-m^2 \pi^2 D_{air} t / 4L^2) \right]$$

208 where $\Delta P_{wl}(t)$ is change in water pressure at time (t), L is the thickness of the vadose zone, D_{air} is the
209 pneumatic diffusivity of the vadose zone. The infinite sum is truncated when the absolute value of an
210 additional term is less than 1×10^{-16} of the starting value. The response function begins at zero and
211 increases to the loading efficiency set to unity and having the following vadose zone parameters: a pneumatic
212 diffusivity of $0.1 \text{ m}^2/\text{s}$ and vadose zone thickness equal to 40 m. The late time values do not represent
213 formation compressibility but the unattenuated air pressure transmission through the vadose zone.

²¹⁴ The well-bore storage kernel was calculated by numerically inverting the Laplace solution of Cooper et al.
²¹⁵ (1967):

$$\Delta P_{wl}(t) = \frac{r_s S K_0(r_w q)}{T q [r_s q K_0(r_s q) + 2\alpha K_0(r_s q)]}$$

²¹⁶ where

$$q = \sqrt{pS/T}$$

²¹⁷ and

$$\alpha = r_s^2 S / r_w^2$$

²¹⁸ where r_s and r_w are the screen and well radii, S is the storativity, T is the transmissivity, K_0 is the modified
²¹⁹ Bessel function of the second kind and order 0, and p is the Laplace transform variable. The following well
²²⁰ and aquifer parameters are used in the Cooper et al. (1967) model to generate the response kernel: radius
²²¹ of the well and screen equal to 0.10 m, aquifer storativity equal to 1×10^{-5} m/m, transmissivity equal to
²²² 5×10^{-4} m²/s.

²²³ The combined response kernel contains the vadose air flow and the well-bore storage models and is
²²⁴ stylistically similar to response functions calculated for field data with both short (seconds to minutes)
²²⁵ and long (hours to days) duration components. The synthetic water pressures and the associated response
²²⁶ functions in the time and frequency domains are presented in Figure 2.

227 *Field Application*

228 Barometric pressure and well water pressures were collected from a fractured rock study site located near
229 Simi, California with monitoring wells completed in the Upper Cretaceous Chatsworth formation consisting
230 of a turbidite sequence of sandstones and interbedded siltstones and shales (Colburn et al., 1981; Link
231 et al., 1984; Cilona et al., 2016). During the analysis period between 2016-08-18 and 2016-10-13, barometric
232 loading, Earth tides, earthquakes, and a recession following precipitation were the dominant signals present
233 in water levels. The monitoring wells were open to the atmosphere and instrumented with a RBRsoloD
234 pressure transducer (non-vented) reporting a sub-millimeter precision (0.0002 decibar which is ~0.0002
235 meter freshwater) (<https://rbr-global.com/products/compact-loggers/rbrsolo-d>). All pressures in
236 decibar were converted to an equivalent pressure head using 1.02 meter freshwater per decibar. Transducers
237 were set to record pressure every second and typically placed ten meters below the well water level. Table
238 1 presents the well construction details for the monitoring wells in this paper. Barometric pressure was
239 measured in RD-130 using a transducer located approximately five meters below top of casing (above the
240 well water level) to avoid large fluctuations in temperature. This well also contained a pressure transducer
241 in the water column and was used to evaluate the distributed lag model and calculate transmissivity and
242 vadose zone pneumatic diffusivity. Responses from two well pairs (C-03, RD-45B and RD-77, RD-121) each
243 separated by approximately one hundred meters are compared to examine spatial variability and similarity
244 of the barometric response (Figure 3).

245 *Barometric Pressure*

246 Barometric pressure is often assumed to be spatially constant at the field site scale. To assess this
247 assumption, two weeks of barometric pressure data from four sensors located in three wells are compared by
248 calculating the time domain response functions. Two transducers were placed in the air column of RD-130
249 at depths of ~5 m bgs (shallow), and 35 m bgs (deep), and the other transducers were located in the air
250 columns of wells RD-08 (~5 m bgs) and RD-10 (~5 m bgs) which are separated from RD-130 by 3000 m and
251 700 m respectively.

252 *Data Processing*

253 A 56 day period between 2016-08-18 and 2016-10-13 was chosen for analysis as precipitation events,
254 sampling, and earthquakes responses (based on United States Geological (USGS) Earthquakes Hazards
255 Program catalog (Survey, 2019)) were expected to be minimal during that time period (Figure 4). The
256 selected period minimized the presence of water level perturbations but is long enough to separate the

257 primary Earth tide components. For this study we focus on pressure changes, and the mean is removed
258 from each data set to improve the visual comparison of values. No other data processing was performed
259 before the application of the regression models.

260 *Response Calculation*

261 The following methods were applied to calculate the static loading efficiency for the synthetic data sets:
262 (1) Ordinary least squares (lag free model of barometric and water pressure); (2) Clark (1967) method
263 using differences calculated between observations spaced 1 hour and 1 day apart; (3) and the Acworth et al.
264 (2016) method with zero Earth tide component (amplitude ratio for 2 cycles per day). To demonstrate the
265 computational efficiency and accuracy of the distributed lag method relative to regular and irregular spaced
266 regression deconvolution models, we tested the three techniques on a 2.5 day noise free synthetic data set
267 that combined vadose and well-bore storage models (Figure 2).

268 The distributed lag and static loading efficiency methods are applied to the field data from RD-130
269 (Figure 4). Prior to the static loading efficiency calculations, the barometric and water pressures were
270 linearly detrended. The Acworth et al. (2016) method included the Earth tide component determined using
271 the *earhtide* package which is an R port of Eterna 3.4 (Kennel and Parker, 2019; Wenzel, 1998). For the time
272 domain distributed lag model, Earth tides were included as wave groups including satellite tidal constituents
273 and not single frequencies (harmonic least squares) (Foreman and Henry, 1989). For the frequency domain
274 response function the complete Hartmann and Wenzel (1995) catalog was used to generate the volumetric
275 strain due to Earth tides (Figure 4). All examples are presented in terms of loading responses, i.e., absolute
276 pressure heads. The response function methods are also calculated with the following levels of subsetting to
277 explore how downsampling can affect the results: 60, 900, 3600, 7200 seconds. Following the application to
278 RD-130 we apply the distributed lag model to two unconfined wells (RD-77, RD-121) and two semi-confined
279 wells (C-03, RD-45B) (Figure 3).

280 Four regressor groups were simultaneously fit to the data in the distributed lag model: global intercept,
281 barometric/loading response, Earth tide response, and the background trend. The global intercept accounts
282 for the different mean values between the water level and barometric measurements. The barometric/loading
283 response is calculated using the distributed lag model presented above. Earth tides (volumetric strain) are
284 calculated in the regression model using harmonic analysis of wave groups simulated with the *R earhtide*
285 package (Kennel and Parker, 2019) and compared to theoretical equilibrium amplitude ratios (Hartmann
286 and Wenzel, 1995). The close coupling of the *hydrorecipes* and *earhtide* packages simplifies the method
287 to obtain amplitude and phase information from water level data sets at multiple frequencies. This is an

288 extension of the Rasmussen and Mote (2007) method to use wave groups instead of specified frequencies
289 which allows for the inclusion constituents with nearby frequencies (e.g. K_1 , P_1 and K_2 , S_2) in the regression
290 as is commonly done in oceanography (Tamura et al., 2007; Foreman et al., 2009; Wenzel, 1998). The number
291 of wave groups is typically chosen based on the equipment precision and the time span of the input data sets
292 that is directly related to resolving different frequency components (Tamura et al., 2007; Foreman et al.,
293 2009). The trend is calculated using natural cubic splines with 27 degrees of freedom. Barometric pressure,
294 water pressure, and synthetic Earth tides are presented in Figure 4.

295 *Parameter estimation.* Parameters were estimated by fitting a combined vadose zone (Weeks, 1979) and
296 well-bore storage model (Cooper et al., 1967) to the distributed lag response in RD-130. The model was
297 scaled using the loading efficiency and an offset term to account for attenuation in the vadose zone. The
298 storativity of the aquifer was fixed at 5.0×10^{-6} m/m and the model fit the following: the vadose zone
299 thickness, the air diffusivity of the vadose zone, the transmissivity of the aquifer, the loading efficiency,
300 and the attenuation term. The parameters were fit using non-linear least squares with the Gauss-Newton
301 algorithm (Hastie, 2017). The first thirty seconds of the response were excluded in the model fit as it is not
302 likely representative of the formation response (low signal to noise).

303 Results

304 Static response for synthetic data

305 Table 2 and Figure 2 compare the results of the static methods applied to the synthetic data representing
306 confined, unconfined and well-bore storage scenarios. For the confined example with no well-bore storage,
307 all methods successfully reproduce the loading efficiency value; however, for well-aquifer combinations with
308 lagged or frequency dependent responses as presented in Figure 2, the estimated barometric or loading
309 efficiency requires additional context to interpret. The response time of a system is often not known a
310 priori, and a single value provides minimal context about the time dependent nature of a response. It is
311 important to note that these are based on noise free data with no external signals and highlights a key
312 deficiency of single valued methods when applied outside their intended use. This is particularly evident
313 in methods that rely on calculating differences between measurements such as Clark's method or have a
314 frequency dependence such as the Acworth method which is typically focused on 1 or 2 (diurnal and semi-
315 diurnal) cycles per day. The performance of a method is linked to the underground and monitoring setup
316 and we have applied these methods outside of their intended use, but unfortunately this is commonly done
317 in practice, and a single value provides limited information to assess the applicability of the method.

318 *Time Domain Methods on Synthetic Data Set*

319 Using the combined well-bore storage and vadose zone synthetic response, regular, irregular and dis-
320 tributed lag models were compared. The computational requirements and model fit to the known solution
321 are presented in Table 3. All methods used the base R *lm* function to solve the multiple linear regression
322 problem in R (R Core Team, 2024), however, alternative methods can be used to solve the system of equa-
323 tions. The regular lag model was calculated by decimating the full 1 second data set into 15 second, 10
324 minute, and 1 hour subsets. The regular lag model quickly reached computational limits both in execution
325 time and memory even when applied to a short time period (~1.5 days). One day is lost from the original
326 2.5 days because the maximum time lag used was one day. Calculating the response function for the full 1
327 second data set either requires changing the method, the solver, or having a powerful computer and patience.
328 For the irregular lag model, the full 1 second data set could be used, and the number of logarithmically
329 spaced lags was varied between 20 and 400 terms. The one hundred term model visually matches the syn-
330 thetic response. For data sets of (millions of observations) the method may be hardware limited due to the
331 large number of terms and observations. The distributed lag model with the full 1 second data set used
332 15 to 25 logarithmically spaced knots. This method outperformed the regular and irregular lag methods in
333 computation time, memory consumption and accuracy. If the input (barometric pressure) is measured at a
334 higher rate than the output (water pressure) it is possible to generate the lagged regressors using the higher
335 frequency inputs at each output time. This approach can also be accomplished by subsetting the output
336 data set during the lagging process to further reduce the size of the regression model while still resolving
337 the early time response. Generally, we suggest collecting the inputs and outputs at the same frequency,
338 however, collecting the inputs (precipitation, surface water levels, pumping rates, barometric pressure, etc.)
339 at a higher frequency than water pressure can be an efficient use of time and computational resources.

340 *Field application*

341 *Spatially variable barometric pressure*

342 Understanding the barometric pressure input is necessary for the interpretation of water level responses.
343 The distributed lag response between barometric pressure measurements at different locations is presented
344 in Figure 5. The results suggest that barometric pressure should be monitored as close to the monitoring
345 well as possible if high frequency monitoring is being used. At this site, the precision of the transducer
346 and the spatially variable barometric pressure affects the early time (up to a few minutes) response, which
347 may manifest as an artificial time lag or a decrease in gain or phase shift for frequency responses (Figure:

348 5). For the two transducers deployed in the same air column of RD-130 the cumulative response is greater
349 than 90% of the impulse after ten seconds. However, for the locations 700 m (RD-10) and 3000 m (RD-08)
350 away from RD-130, the spatial variability of barometric pressure manifests as a delayed response in the
351 time domain, and a decrease in coherence in the frequency domain at around 100 cycles per day. These
352 differences may be due to both the deployment method in the borehole, differing borehole completions,
353 transducer manufacturing variability (clock drift, sensor sensitivity), the spatial variability of barometric
354 pressure and potentially other factors. At this field site the barometric pressure is temporally variable due
355 to seasonal winds and surface heating that may differentially affect the monitoring locations on site.

356 *Barometric responses (RD-130)*

357 In contrast to the noise free synthetic data sets, field data sets are inherently noisy. To mitigate noise
358 from external signals the analysis time period was selected so that pumping, precipitation and earthquakes
359 effects were minimal. The predominant signals in the water pressure data result from barometric pressure
360 changes (distributed lag), Earth tides (harmonic wave groups) and declining water levels following antecedent
361 precipitation (natural cubic spline). All these signals were included in the loading response function regres-
362 sion model. Loading response functions due to barometric pressure are presented in Figure 6. There are
363 three regions defined by the responses: low signal to noise; well-bore storage; and vadose air flow (Figure
364 6). The duration of these regions are dependent on the monitoring well design, monitoring equipment, and
365 subsurface properties. For this data set the first 10 seconds of lag time of the response is characterized by
366 low signal to noise and is due to a variety of factors, including, the transducer precision, temporal drift of
367 transducers, borehole air flow, time required for aquifer deformation, and potentially non-linearity of the
368 response due to changing borehole and formation conditions. The monitoring frequency has a direct impact
369 on the resulting response functions and for this well a monitoring frequency of 60 seconds is too coarse to
370 estimate the well-bore storage response that is related to the formation transmissivity and well geometry
371 (Figure 6). In addition, the vadose response, used to estimate the pneumatic diffusivity of the vadose zone,
372 is not clearly resolved with a monitoring frequency greater than 900 seconds. The static loading efficiency
373 values presented in Figure 6 are 0.47 (Clark 1 hour), 0.61 (Acworth 2 cpd), 0.85 (Clark 1 day) and 0.83 (least
374 squares). We present this not to advocate one method over another or to suggest the values are in error, but
375 to highlight the importance of context when interpreting a single valued response. The appropriate context
376 to understand these differences is available via the response functions.

377 Four visual checks were made to evaluate the quality of the barometric/loading response functions using
378 the distributed lag method (Figure 6). First, it is assumed that the barometric/loading response function

379 should be smoothly varying and jagged or large oscillations in the response suggest the presence of unac-
380 counted for noise or trends in the data, potential error in the analysis, or a more complex barometric/loading
381 response than commonly predicted. Second, the frequency response function method and the distributed lag
382 methods should give similar results. Third, Earth tide amplitude ratios determined using harmonic analysis
383 should be similar to theoretical amplitude ratios. Finally, residuals should have a random pattern centered
384 on zero and should not be much larger than transducer precision. A closer examination of items 3 and 4 is
385 presented below.

386 *Signal decomposition*

387 Figure 7 presents the input data sets and the signal decomposition obtained from the distributed lag
388 model (barometric pressure component, Earth tide component, and spline component). Absolute residuals
389 from the model fit are generally near the transducer resolution of ~0.02 cm water. Remaining structure
390 (time periods of large residuals or biased positive/negative) in the residuals is likely the result of seismicity,
391 temporal offsets between transducers (clock drift), air flow between vadose zone and borehole, and other
392 stresses or physical changes not accounted for in the model. Earth tides are measurable but have amplitudes
393 less than 0.05 cm freshwater and have ratios consistent with the theoretical ratios from the Hartmann and
394 Wenzel (1995) catalog (Figure 7). Even though these amplitudes are near the instrument precision the
395 relative amplitudes of tidal constituents match theory. This suggests that the majority of the barometric
396 pressure component was effectively removed (i.e. the removal of the barometric pressure component allowed
397 the Earth tide component to be quantified). If existing barometric signal was present the relative magnitudes
398 of the Earth tide components would likely differ from theory particularly at the S₂ and K₁ frequencies. The
399 diurnal (nominally one cycle per day) differences from the theoretical tides may result from local variability
400 of tidal signals, ocean loading, the presence of additional diurnal forcings not accounted for in the model
401 such as evapotranspiration, or the incomplete removal of the barometric signal due to non-linearities of the
402 response.

403 *Spatially variable barometric responses*

404 Barometric responses from an unconfined well pair (RD-77 and RD-121) and a semi-confined well pair
405 (RD-45B and C-03) are compared to examine spatial variability (Figures 8 and 9). At this site it is expected
406 that the timing of the lagged response is related to investigation scale: early time corresponds to local
407 properties; and late time corresponds to larger scale properties (>100 m). The responses for the well pairs
408 support this expectation as each well in the well pair has a unique early response, however, at late time they

409 collapse to the same values suggesting the same controlling features or mechanisms. Conceptually this is
410 consistent with the early time response being related to well-bore storage, a response dependent on the local
411 formation transmissivity (or well skin) and borehole geometry. At this site, the late time response will be
412 governed by different components of the subsurface for the unconfined and semi-confined wells. Specifically,
413 the unconfined wells are more sensitive to vadose zone properties (water saturation, pneumatic diffusivity)
414 and the semi-confined wells will be more sensitive to confining layer properties (vertical diffusivity).

415 The unconfined and semi-confined responses can be interpreted to better understand the continuity of
416 subsurface properties (Figure 8). The water level elevation for the unconfined wells (RD-77 and RD-121) is
417 roughly the same, however, the vadose zone is 13 meters thicker at RD-121 than RD-77. Assuming vertical
418 air flow and the same pneumatic diffusivity, the thicker vadose zone would lead to a delayed response
419 at RD-121 relative to RD-77. The two responses converge after ~12 hours (0.5 cycles per day) and are
420 attenuated by a similar magnitude (Figure 8). The value of the response at 1.5 days for both wells is 0.68
421 suggesting a similar mechanism is governing the value. We expect that this late time value is primarily due
422 to capillary fringe attenuation highlighted by Evans et al. (1991), which could be considered similar between
423 the monitoring wells. The semi-confined response is indistinguishable after time lags of 1 hour (~7 cycles
424 per day). This suggests that the semi-confining layer has continuity and similar properties in the vicinity
425 of the monitoring wells. Cumulative responses for each well are based on independent water level data and
426 the close similarity at late time provides additional confidence in the results.

427 Figure 9 displays the responses from the five water pressure data sets. After barometric pressure, Earth
428 tide and background trend components are removed from the water pressure data, small seismic events are
429 clearly visible in the residuals from the model fit (RD-45B in particular). The general lack of structure in the
430 residuals, which are near instrument precision, further supports the quality of the regression deconvolution
431 method with distributed lags and harmonic Earth tide constituents.

432 *Parameter estimation*

433 Following the determination of a response function, an interpretive model can be fit to estimate subsurface
434 properties. The combined Weeks (1979) and Cooper et al. (1967) model was applied to the time domain
435 response function for RD-130. The model fit for RD-130 is presented in Figure 10. The first 30 seconds
436 of response were excluded as it is characterized by a low signal to noise ratio. While the fit is far from
437 perfect using this model applied to a fractured, folded and faulted system, the result suggests that given
438 high frequency data it is possible to extend the range of transmissivity estimates from barometric/loading
439 responses to greater than $\sim 1 \times 10^{-4} \text{ m}^2/\text{s}$ as was noted as a practical limitation in Spane (2002). Without the

440 high frequency barometric data set it would not have been possible to estimate the transmissivity from the
441 water level response as the system responds too rapidly relative to the observation frequency. Unfortunately,
442 there is no independent transmissivity measurement for RD-130 so the validity of this estimate remains
443 uncertain. The result of $5 \times 10^{-4} \text{ m}^2/\text{s}$ lies in the upper range of transmissivities presented in Allègre et al.
444 (2016) for the site. The value of air diffusivity of $0.13 \text{ m}^2/\text{s}$ is in the range presented by Spane (2002). The
445 relatively simple model is unable to perfectly represent the empirically derived response and demonstrates
446 the need for further work to characterize the complexity imparted by these fractured and faulted systems.
447 This complexity may be the result of multiple pathways of pressure migration through the vadose zone
448 (fractures vs. faults vs. matrix) and spatial variability of hydraulic conductivity and storativity.

449 **Summary and Conclusions**

450 This paper presents an improved method of determining the water level response following a series of
451 barometric pressure changes in the presence of Earth tides and background trends at high frequency (i.e. 1
452 second data) now technologically practical. The distributed lag method scales to data sets with millions
453 of observations and long maximum lag times (multiple days). Given the appropriate monitoring strategy,
454 water and barometric pressures coherence values of ~0.8 at one thousand cycles per day were obtained, an
455 extension of two orders of magnitude from currently presented examples. This effectively allows for the
456 quantitation of formation responses that occur rapidly and has a direct influence on the increasing range
457 of hydraulic diffusivities and therefore, higher transmissivities can be estimated. Multiple components
458 of the hydrogeologic system are characterized from a single barometric/loading response function as the
459 barometric pressure changes result in stress changes that travel through different portions of the subsurface
460 and at different rates. Site specific conditions determine response times and at this site the early time
461 response is governed by local well conditions and the late time is related to larger scale characteristics such
462 as vadose zone conditions and confining layer properties. The single valued barometric efficiency was shown
463 to be ill-suited to evaluating these types of lagged responses.

464 The typical frequency for ambient monitoring of water levels in hydrogeologic and geotechnical investi-
465 gations is a few minutes to hours, and the choice is based on historical practice, instrument specifications,
466 signal to noise ratio, power consumption, data storage and processing capabilities. In practice, the moni-
467 toring frequency is rarely selected based on the formation and well properties. Hendry et al. (2018) suggest
468 that intervals less than thirty minutes may be useful and shorter measurement intervals are better. Fortu-
469 nately, the ability to record water pressure changes at high frequency and precision is possible with little
470 additional effort. Combined with increasing computational capabilities and software advancements, data
471 sets with millions of observations can be analyzed on a mid-range laptop. This paper focused on barometric
472 responses; however, the distributed lag method is applicable to other signals such as variable rate pumping,
473 surface water levels, and precipitation. All methods mentioned in this paper have been implemented in
474 the actively developed open source *R* software package *hydrorecipes* creating a consistent framework for the
475 analysis of groundwater level/pressure responses to barometric pressure (and other) signals.

476 **Acknowledgements**

477 Funding was provided by The Boeing Company and the Natural Science and Engineering Research
478 Council of Canada Industrial Research Chair grant to Dr. B.L. Parker (IRC 363783-11 and IRC 363783-18).

⁴⁷⁹ We would like to thank Ryan Kroeker of the University of Guelph for help in the field. Dr. Jonathan Munn,
⁴⁸⁰ Dr. Carlos Maldaner, Dr. Todd Rasmussen, Dr. Emmanuelle Arnaud, Dr. John Cherry, and Ann Garniss
⁴⁸¹ for valuable comments on the draft manuscript and thesis. The idea for using distributed lag models was
⁴⁸² inspired by the R dlnm package written by Dr. Antonio Gasparrini.

483 **References**

- 484 Acworth, R.I., Halloran, L.J., Rau, G.C., Cuthbert, M.O., Bernardi, T.L., 2016. An objective frequency domain method for
485 quantifying confined aquifer compressible storage using Earth and atmospheric tides. *Geophysical Research Letters* 43,
486 11,671–11,678. doi:10.1002/2016GL071328.
- 487 Allègre, V., Brodsky, E.E., Xue, L., Nale, S.M., Parker, B.L., Cherry, J.A., 2016. Using earth-tide induced water pressure
488 changes to measure in situ permeability: A comparison with long-term pumping tests. *Water Resources Research* 52,
489 3113–3126. doi:10.1002/2015WR017346.
- 490 Almon, S., 1965. The Distributed Lag Between Capital Appropriations and Expenditures. *Econometrica* 33, 178. doi:10.2307/
491 1911894.
- 492 Bohling, G.C., Jin, W., Butler, J.J., 2011. Kansas Geological Survey Kansas Geological Survey Barometric Response Function
493 Software User's Guide. Technical Report. Kansas Geological Survey. URL: www.kgs.ku.edu.
- 494 Butler, J.J., Jin, W., Mohammed, G.A., Reboulet, E.C., 2011. New insights from well responses to fluctuations in barometric
495 pressure. *Ground Water* doi:10.1111/j.1745-6584.2010.00768.x.
- 496 Cilona, A., Aydin, A., Likerman, J., Parker, B., Cherry, J., 2016. Structural and statistical characterization of joints and
497 multi-scale faults in an alternating sandstone and shale turbidite sequence at the santa susana field laboratory: Implications
498 for their effects on groundwater flow and contaminant transport. *Journal of Structural Geology* 85, 95–114.
- 499 Clark, W.E., 1967. Computing the barometric efficiency of a well. *Journal of the Hydraulics Division* 93, 93–98.
- 500 Colburn, I.P., Saul, L.E.R., Almgren, A., 1981. The chatsworth formation: a new formation name for the upper cretaceous
501 strata of the simi hills, california .
- 502 Cooper, H.H., Bredehoeft, J.D., Papadopoulos, I.S., 1967. Response of a finite-diameter well to an instantaneous charge of
503 water. *Water Resources Research* 3, 263–269.
- 504 Davis, D.R., Rasmussen, T.C., 1993. A Comparison of Linear Regression With Clark's Method for Estimating Barometric
505 Efficiency of Confined Aquifers. *Water Resources Research* 29, 1849–1854.
- 506 Evans, K., Beavan, J., Simpson, D., Mousa, S., 1991. Estimating aquifer parameters from analysis of forced fluctuations in
507 well level: An example from the nubian formation near aswan, egypt: 3. diffusivity estimates for saturated and unsaturated
508 zones. *Journal of Geophysical Research: Solid Earth* 96, 12161–12191.
- 509 Foreman, M., Henry, R., 1989. The harmonic analysis of tidal model time series. *Advances in Water Resources* 12, 109–120.
510 URL: <https://linkinghub.elsevier.com/retrieve/pii/0309170889900171>, doi:10.1016/0309-1708(89)90017-1.
- 511 Foreman, M.G.G., Cherniawsky, J.Y., Ballantyne, V.A., 2009. Versatile Harmonic Tidal Analysis: Improvements and Appli-
512 cations. *Journal of Atmospheric and Oceanic Technology* 26, 806–817. doi:10.1175/2008JTECH0615.1.
- 513 Furbish, D.J., 1991. The response of water level in a well to a time series of atmospheric loading under confined conditions.
514 *Water Resources Research* 27, 557–568. doi:10.1029/90WR02775.
- 515 Gasparri, A., 2011. Distributed Lag Linear and Non-Linear Models in R: The Package dlnm. *Journal of statistical software*
516 43, 1–20.
- 517 Gonthier, G.J., 2007. A graphical method for estimation of barometric efficiency from continuous data—concepts and application
518 to a site in the piedmont. *Air Force Plant* 6.
- 519 Hartmann, T., Wenzel, H.G., 1995. The HW95 tidal potential catalogue. *Geophysical Research Letters* 22, 3553–3556.
520 doi:10.1029/95GL03324.
- 521 Hastie, T.J., 2017. Statistical models in S. Routledge.

- 522 Haugh, L.D., Box, G.E.P., 1977. Identification of Dynamic Regression (Distributed Lag) Models Connecting Two Time Series.
 523 Journal of the American Statistical Association 72, 121. doi:10.2307/2286919.
- 524 Hendry, M.T., Smith, L.A., Hendry, M.J., 2018. Analysis of measured pore pressure response to atmospheric pressure changes
 525 to evaluate small-strain moduli: methodology and case studies. Canadian Geotechnical Journal 55, 1248–1256. doi:10.1139/
 526 cgj-2016-0584.
- 527 Hussein, M.E.A., Odling, N.E., Clark, R.A., 2013. Borehole water level response to barometric pressure as an indicator of
 528 aquifer vulnerability. Water Resources Research 49, 7102–7119. doi:10.1002/2013WR014134.
- 529 Hvorslev, M.J., 1951. Time lag and soil permeability in ground-water observations. 36, Waterways Experiment Station, Corps
 530 of Engineers, US Army.
- 531 Jacob, C.E., 1940. On the flow of water in an elastic artesian aquifer. Transactions, American Geophysical Union 21, 574–586.
- 532 Kennel, J., Parker, B., 2019. earthtide: Parallel Implementation of 'ETERNA 3.40' for Prediction and Analysis of Earth Tides.
 533 URL: <https://cran.r-project.org/web/packages/earthtide/index.html>, doi:10.5281/zenodo.2673048. r package version
 534 0.0.6.
- 535 Kennel, J., Parker, B., 2022. hydrorecipes: Additional Steps for the Analysis of Water Level Data. URL: <https://github.com/jkennel/hydrorecipes>, doi:10.5281/zenodo.6773849. r package version 0.0.4.
- 537 Kuang, X., Jiao, J.J., Li, H., 2013. Review on airflow in unsaturated zones induced by natural forcings. Water Resources
 538 Research 49, 6137–6165. URL: <https://agupubs.onlinelibrary.wiley.com/doi/abs/10.1002/wrcr.20416>, doi:<https://doi.org/10.1002/wrcr.20416>. _eprint: <https://agupubs.onlinelibrary.wiley.com/doi/pdf/10.1002/wrcr.20416>.
- 540 Kuhn, M., Wickham, H., 2022. recipes: Preprocessing and Feature Engineering Steps for Modeling. URL: <https://CRAN.R-project.org/package=recipes>. r package version 1.0.1.
- 542 Lai, G., Ge, H., Wang, W., 2013. Transfer functions of the well-aquifer systems response to atmospheric loading and Earth tide
 543 from low to high-frequency band. Journal of Geophysical Research: Solid Earth 118, 1904–1924. doi:10.1002/jgrb.50165.
- 544 Link, M.H., Squires, R.L., Colburn, I.P., 1984. Slope and deep-sea fan facies and paleogeography of upper cretaceous chatsworth
 545 formation, simi hills, california. AAPG Bulletin 68, 850–873.
- 546 McMillan, T.C., Andersen, M.S., Timms, W., Rau, G.C., 2020. In-situ estimation of subsurface hydro-geomechanical proper-
 547 ties using the groundwater response to Earth and atmospheric tides. URL: <http://www.essoar.org/doi/10.1002/essoar.10505394.1>. archive Location: world Publisher: Earth and Space Science Open Archive
 549 Section: Geophysics.
- 550 Munk, W.H., Cartwright, D.E., 1966. Tidal Spectroscopy and Prediction. Philosophical Transactions of the Royal Society A:
 551 Mathematical, Physical and Engineering Sciences 259, 533–581. doi:10.1098/rsta.1966.0024.
- 552 Odling, N.E., Perulero Serrano, R., Hussein, M.E.A., Riva, M., Guadagnini, A., 2015. Detecting the vulnerability of groundwater
 553 in semi-confined aquifers using barometric response functions. Journal of Hydrology 520, 143–156. doi:10.1016/j.jhydrol.
 554 2014.11.016.
- 555 R Core Team, 2024. R: A Language and Environment for Statistical Computing. R Foundation for Statistical Computing.
 556 Vienna, Austria. URL: <https://www.R-project.org/>.
- 557 Rasmussen, T.C., Crawford, L.A., 1997. Identifying and Removing Barometric Pressure Effects in Confined and Unconfined
 558 Aquifers. Ground Water 35, 502–511. doi:10.1111/j.1745-6584.1997.tb00111.x.
- 559 Rasmussen, T.C., Mote, T.L., 2007. Monitoring surface and subsurface water storage using confined aquifer water levels at the
 560 savannah river site, usa. Vadose Zone Journal 6, 327–335.

- 561 Rau, G.C., Cuthbert, M.O., Acworth, R.I., Blum, P., 2020. Technical note: Disentangling the groundwater response to
 562 Earth and atmospheric tides to improve subsurface characterisation. *Hydrology and Earth System Sciences* 24, 6033–
 563 6046. URL: <https://hess.copernicus.org/articles/24/6033/2020/>, doi:<https://doi.org/10.5194/hess-24-6033-2020>.
 564 publisher: Copernicus GmbH.
- 565 Rau, G.C., McMillan, T.C., Andersen, M.S., Timms, W.A., 2022. In situ estimation of subsurface hydro-geomechanical
 566 properties using the groundwater response to semi-diurnal earth and atmospheric tides. *Hydrology and Earth System
 567 Sciences* 26, 4301–4321.
- 568 Ritzi, R.W., Sorooshian, S., Hsieh, P.A., 1991. The estimation of fluid flow properties from the response of water levels in wells
 569 to the combined atmospheric and Earth tide forces. *Water Resources Research* 27, 883–893. doi:[10.1029/91WR00070](https://doi.org/10.1029/91WR00070).
- 570 Rojstaczer, S., 1988. Determination of fluid flow properties from the response of water levels in wells to atmospheric loading.
 571 *Water Resources Research* 24, 1927–1938. doi:[10.1029/WR024i011p01927](https://doi.org/10.1029/WR024i011p01927).
- 572 Smith, L.A., van der Kamp, G., Hendry, J.M., 2013. A new technique for obtaining high-resolution pore pressure records in
 573 thick claystone aquitards and its use to determine in situ compressibility. *Water Resources Research* 49, 732–743. URL:
 574 <http://doi.wiley.com/10.1002/wrcr.20084>, doi:[10.1002/wrcr.20084](https://doi.org/10.1002/wrcr.20084).
- 575 Spane, F.A., 2002. Considering barometric pressure in groundwater flow investigations. *Water Resources Research* 38, 14–1 to
 576 14–18. doi:[10.1029/2001WR000701](https://doi.org/10.1029/2001WR000701).
- 577 Survey, U.S.G., 2019. Earthquake hazards program catalog. <https://earthquake.usgs.gov/fdsnws/event/1/>. Online; accessed
 578 2019-11-21.
- 579 Tamura, Y., Sato, T., Ooe, M., Ishiguro, M., 2007. A procedure for tidal analysis with a Bayesian information criterion.
 580 *Geophysical Journal International* 104, 507–516. doi:[10.1111/j.1365-246X.1991.tb05697.x](https://doi.org/10.1111/j.1365-246X.1991.tb05697.x).
- 581 Tibshirani, R., 1996. Regression Shrinkage and Selection Via the Lasso. *Journal of the Royal Statistical
 582 Society: Series B (Methodological)* 58, 267–288. URL: <https://rss.onlinelibrary.wiley.com/doi/abs/10.1111/j.2517-6161.1996.tb02080.x>. eprint:
 583 <https://rss.onlinelibrary.wiley.com/doi/pdf/10.1111/j.2517-6161.1996.tb02080.x>.
- 585 Toll, N.J., Rasmussen, T.C., 2007. Removal of barometric pressure effects and earth tides from observed water levels. *Ground
 586 Water* 45, 101–105. doi:[10.1111/j.1745-6584.2006.00254.x](https://doi.org/10.1111/j.1745-6584.2006.00254.x).
- 587 Turnadge, C., Crosbie, R.S., Barron, O., Rau, G.C., 2019. Comparing methods of barometric efficiency characterisation for
 588 specific storage estimation. *Groundwater* .
- 589 Wang, W., Yan, J., 2021. Shape-restricted regression splines with R package splines2. *Journal of Data Science* 19, 498–517.
 590 doi:[10.6339/21-JDS1020](https://doi.org/10.6339/21-JDS1020).
- 591 Wang, W., Yan, J., 2024. splines2: Regression Spline Functions and Classes. URL: <https://CRAN.R-project.org/package=splines2.r> package version 0.5.2.
- 593 Weeks, E.P., 1979. Barometric fluctuations in wells tapping deep unconfined aquifers. *Water Resources Research* 15, 1167–1176.
 594 doi:[10.1029/WR015i005p01167](https://doi.org/10.1029/WR015i005p01167).
- 595 Wenzel, H.G., 1998. Earth Tide Data Processing Package ETERNA 3.30: The Nanogal Software. *Proceedings of the Interna-
 596 tional Symposium on Earth Tides* , 487–494URL: <http://www.eas.slu.edu/GGP/ETERNA34/MANUAL/ETERNA33.HTM>.
- 597 Yang, H., Shibata, T., 2020. Aquifer classification and pneumatic diffusivity estimation using periodic groundwater level
 598 changes induced by barometric pressure. *Hydrological Research Letters* 14, 111–116. doi:[10.3178/hrl.14.111](https://doi.org/10.3178/hrl.14.111).

599 **List of Figures**

- 600 1 A barometric pressure change can induce flow that is governed by the diffusivity of different
601 portions of the subsurface. The lag time or frequency dependence of the barometric response
602 is related to different components of the system. In some cases, the responses of multiple
603 components of the system will occur contemporaneously and for others they can be separated
604 into distinct regions of the response. D_{local} is the diffusivity of the well skin, $D_{aquifer}$ is the
605 diffusivity of the aquifer, D'_{conf} is the vertical diffusivity of the confining layer, D'_{unconf} is the
606 vertical diffusivity of the unconfined aquifer, D_{air} is the pneumatic diffusivity of the vadose
607 zone. 26
- 608 2 Field observed barometric pressure data was convolved with the response functions to generate
609 synthetic water pressures to generate synthetic loading response functions. The synthetic
610 water pressures resulting from the convolution of barometric pressure and the response kernels
611 are shown on the left. Response functions (kernels) with the following parameters were applied
612 to the barometric pressure data: Confined (LE = 0.38); Vadose (pneumatic diffusivity = 0.1
613 m²/s and vadose thickness = 40 m); Storage (transmissivity = 5×10^{-4} m²/s and well diameter
614 = 0.1 m). The frequency and time domain responses show similarities, with the early time
615 response corresponding to high frequencies, and the late time response corresponding to low
616 frequencies. Results from the least squares, Clark's, and Acworth methods using the synthetic
617 water pressures and input barometric pressure are presented on the response figures. 27
- 618 3 Locations of the barometric pressure sensor and well pairs for the field comparison. RD-130
619 contains pressure transducers in the air column and submerged in the water column. The
620 well pairs (C-03 and RD-45B, RD-77 and RD-121) were selected to highlight similarities and
621 differences of the barometric response. Barometric pressure from RD-130 is used for all the
622 water pressure barometric response functions. Aerial imagery courtesy of the U.S. Geological
623 Survey Earth Explorer (Digital Mapping Inc., 2008). 28
- 624 4 Time and frequency domain representations of the barometric and detrended water pressure
625 for the field evaluation of well RD-130. There are a few salient points about the frequency
626 domain representation. First, the amplitude spectra for barometric pressure is larger than
627 the respective values for water pressure. The main exception to this is at the M_2 frequency
628 where the water level contains a measurable but small Earth tide signal. Second, the ratio of
629 amplitudes (water/barometric) varies as a function of frequency and shows a steady decline
630 with increasing frequency. In the absence of other signals, the ratio of the amplitude of the
631 water pressure to the barometric pressure can give an idea of the frequency dependent loading
632 efficiency. 29
- 633 5 Comparison of barometric responses from different locations on site. In the time domain
634 a constant response of 1.0 would suggest the same barometric signal at different locations.
635 Lateral and vertical variability of barometric pressure results in deviations from the ideal
636 scenario. The high frequency measurements allow for the spatial variability of barometric
637 pressure to be quantified and demonstrates early time variability. The two transducers in
638 the air column of RD-130 show a cumulative response that rapidly approaches 1.0 and are
639 coherent to greater than 1000 cycles per day. At early times the spatial variability of air
640 pressure caused by both local well completions and barometric pressure differences may limit
641 the usefulness of results. In the frequency domain plot, the coherence drops off for transducers
642 separated by lateral and vertical distances. The coherence (a measure of similarity) between
643 the submerged transducer (RD-130 Water) and the transducer in the air column (RD-130
644 Shallow) is also presented to highlight the extended analysis range that is possible. 30

645	6	Cumulative loading response for RD-130 determined using the multiple linear regression model. There are three main regions of response for this unconfined well. The first ten seconds of lag corresponds to a low signal to noise response. This portion of the data likely does not represent the well-formation response. The next portion of the response corresponds to well-bore storage and lasts until around 300 seconds, and the final portion of the response corresponds to vadose air flow.	31
651	7	Barometric pressure, background trend, and Earth tide components determined from the multiple linear regression model. The background trend, which is approximated with natural splines, could likely have been fit with a linear trend in this example. For the frequency domain representation we focus on the diurnal and semi-diurnal frequencies (one and two cycles per day). In the frequency domain Earth tide component facet the purple dashes are the theoretical equilibrium tidal amplitudes and the grey bars were determined from harmonic wave group analysis in the regression model. The theoretical Earth tide amplitudes are scaled values from the Hartmann and Wenzel (1995) catalog. The Earth tide amplitudes show excellent agreement with the semi-diurnal tidal groups, but there is some additional noise that may be present at the diurnal frequencies possibly due to ocean loading, evapotranspiration, or other signals not considered in the model. Note the scale difference for the Earth tide and residuals.	32
663	8	Comparison of well pairs (C-03 and RD-45B, RD-77 and RD-121). At early times each well has a unique response, but at late times the responses are indistinguishable for the well pairs.	33
665	9	Summary of distributed lag model fits, Earth tide components and the residuals from the model fit. Given the proximity to the barometric pressure monitor, RD-130 provides the signal to noise ratio for the early time response. For RD-130, RD-77, and RD-121 which are considered unconfined, the Earth tide response is close to instrument precision and therefore increased uncertainty is associated with the values. C-03 and RD-45B are semi-confined and have Earth tide ratios between components that are consistent with theory providing increased confidence in the characterization. In general, the residuals are close to instrument precision with the largest residuals being associated with seismicity, which was not included in the regression model.	34
674	10	Response function determined with the distributed lag model and the combined well-bore storage and vadose air flow model fit. Parameters were fit using non-linear least squares with the Gauss-Newton algorithm. Some of the differences may be related to heterogeneity in the vadose zone resulting from faults and fractures.	35

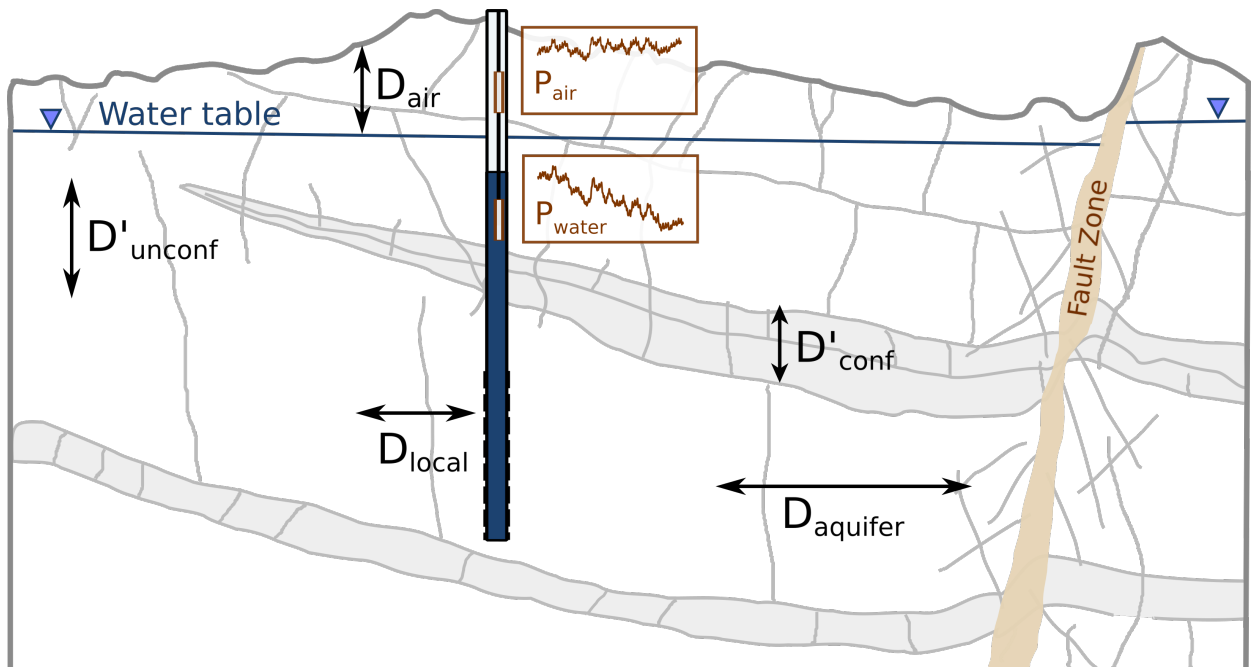


Figure 1: A barometric pressure change can induce flow that is governed by the diffusivity of different portions of the subsurface. The lag time or frequency dependence of the barometric response is related to different components of the system. In some cases, the responses of multiple components of the system will occur contemporaneously and for others they can be separated into distinct regions of the response. D_{local} is the diffusivity of the well skin, $D_{aquifer}$ is the diffusivity of the aquifer, D'_{conf} is the vertical diffusivity of the confining layer, D'_{unconf} is the vertical diffusivity of the unconfined aquifer, D_{air} is the pneumatic diffusivity of the vadose zone.

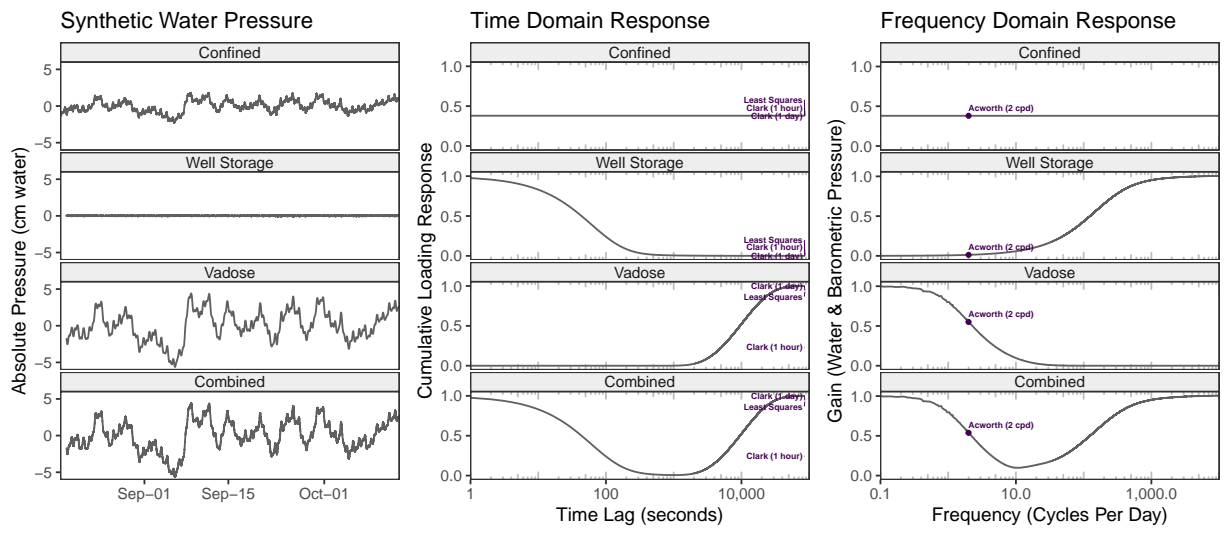


Figure 2: Field observed barometric pressure data was convolved with the response functions to generate synthetic water pressures resulting from the convolution of barometric pressure and the response kernels are shown on the left. Response functions (kernels) with the following parameters were applied to the barometric pressure data: Confined ($LE = 0.38$); Vadose (pneumatic diffusivity = $0.1 \text{ m}^2/\text{s}$ and vadose thickness = 40 m); Storage (transmissivity = $5 \times 10^{-4} \text{ m}^2/\text{s}$ and well diameter = 0.1 m). The frequency and time domain responses show similarities, with the early time response corresponding to high frequencies, and the late time response corresponding to low frequencies. Results from the least squares, Clark's, and Acworth methods using the synthetic water pressures and input barometric pressure are presented on the response figures.

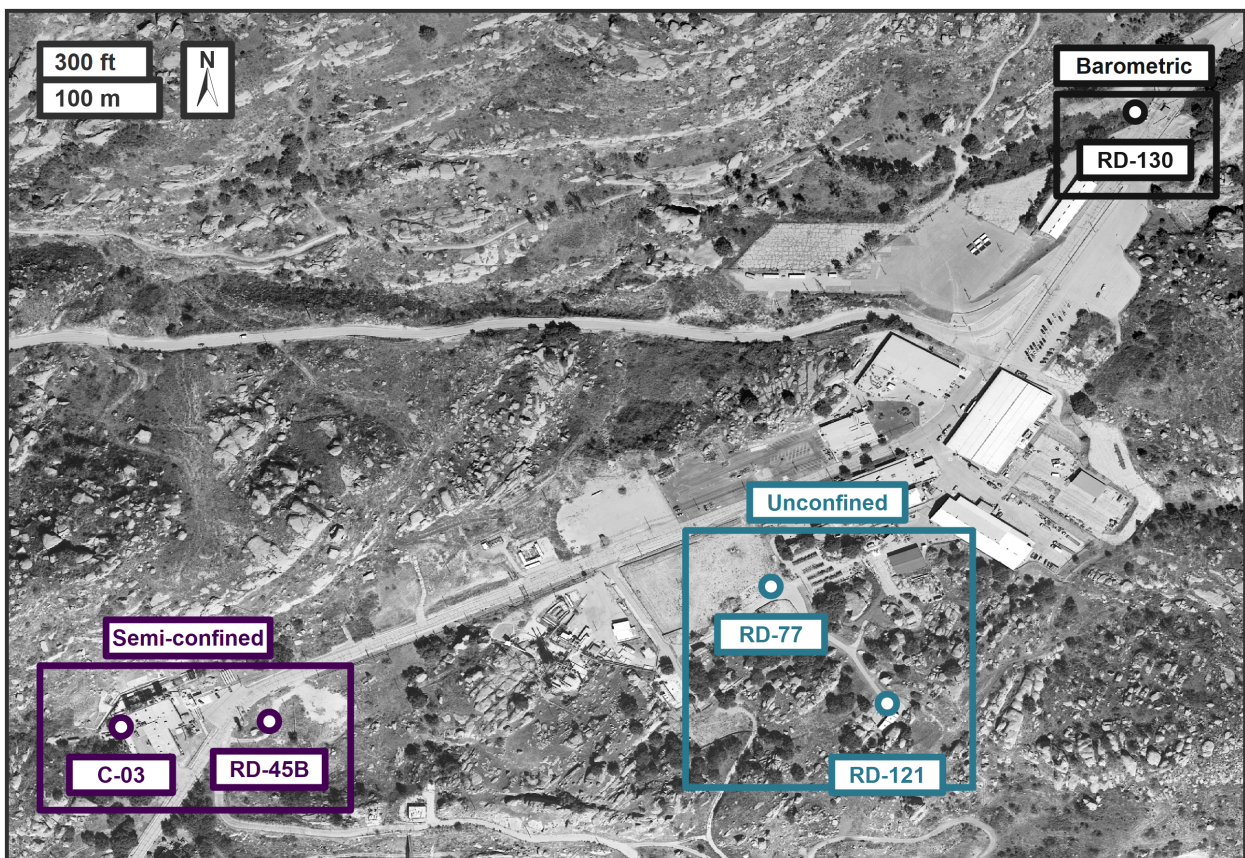


Figure 3: Locations of the barometric pressure sensor and well pairs for the field comparison. RD-130 contains pressure transducers in the air column and submerged in the water column. The well pairs (C-03 and RD-45B, RD-77 and RD-121) were selected to highlight similarities and differences of the barometric response. Barometric pressure from RD-130 is used for all the water pressure barometric response functions. Aerial imagery courtesy of the U.S. Geological Survey Earth Explorer (Digital Mapping Inc., 2008).

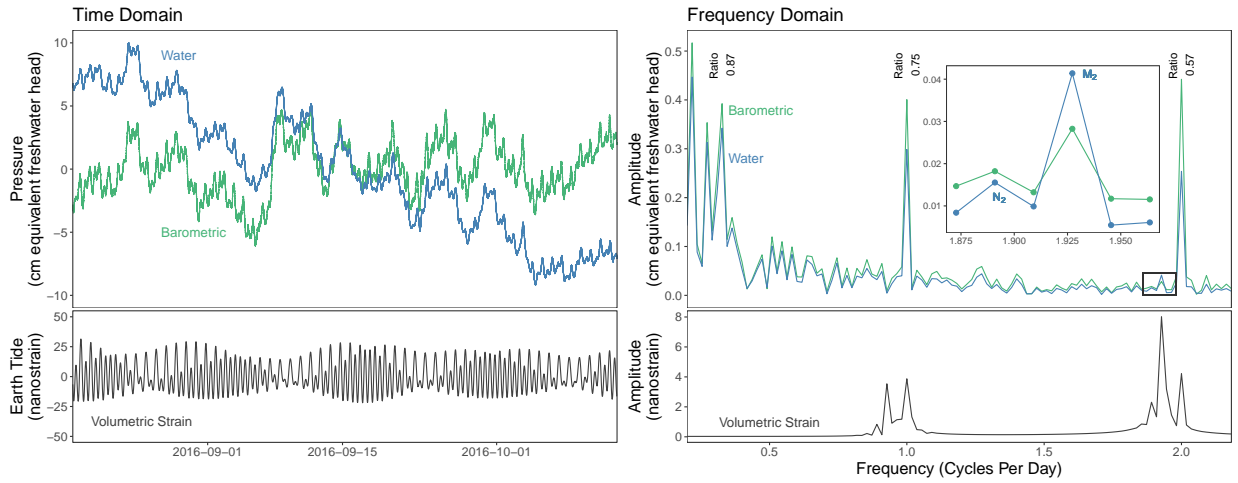


Figure 4: Time and frequency domain representations of the barometric and detrended water pressure for the field evaluation of well RD-130. There are a few salient points about the frequency domain representation. First, the amplitude spectra for barometric pressure is larger than the respective values for water pressure. The main exception to this is at the M_2 frequency where the water level contains a measurable but small Earth tide signal. Second, the ratio of amplitudes (water/barometric) varies as a function of frequency and shows a steady decline with increasing frequency. In the absence of other signals, the ratio of the amplitude of the water pressure to the barometric pressure can give an idea of the frequency dependent loading efficiency.

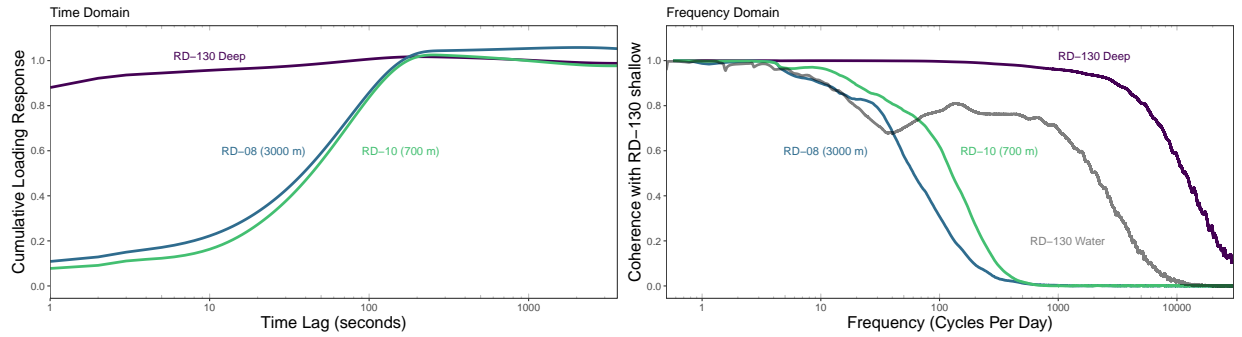


Figure 5: Comparison of barometric responses from different locations on site. In the time domain a constant response of 1.0 would suggest the same barometric signal at different locations. Lateral and vertical variability of barometric pressure results in deviations from the ideal scenario. The high frequency measurements allow for the spatial variability of barometric pressure to be quantified and demonstrates early time variability. The two transducers in the air column of RD-130 show a cumulative response that rapidly approaches 1.0 and are coherent to greater than 1000 cycles per day. At early times the spatial variability of air pressure caused by both local well completions and barometric pressure differences may limit the usefulness of results. In the frequency domain plot, the coherence drops off for transducers separated by lateral and vertical distances. The coherence (a measure of similarity) between the submerged transducer (RD-130 Water) and the transducer in the air column (RD-130 Shallow) is also presented to highlight the extended analysis range that is possible.

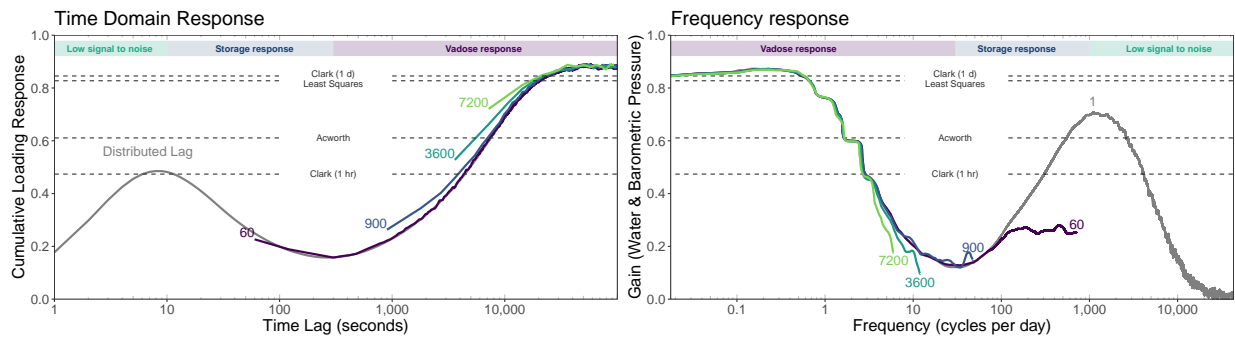


Figure 6: Cumulative loading response for RD-130 determined using the multiple linear regression model. There are three main regions of response for this unconfined well. The first ten seconds of lag corresponds to a low signal to noise response. This portion of the data likely does not represent the well-formation response. The next portion of the response corresponds to well-bore storage and lasts until around 300 seconds, and the final portion of the response corresponds to vadose air flow.

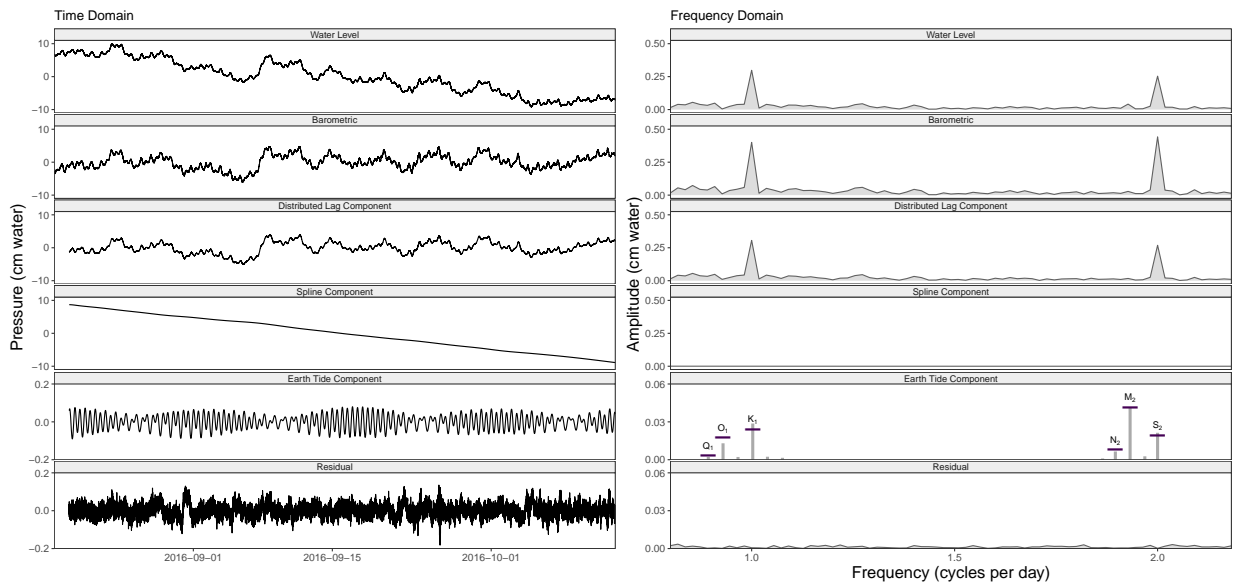


Figure 7: Barometric pressure, background trend, and Earth tide components determined from the multiple linear regression model. The background trend, which is approximated with natural splines, could likely have been fit with a linear trend in this example. For the frequency domain representation we focus on the diurnal and semi-diurnal frequencies (one and two cycles per day). In the frequency domain Earth tide component facet the purple dashes are the theoretical equilibrium tidal amplitudes and the grey bars were determined from harmonic wave group analysis in the regression model. The theoretical Earth tide amplitudes are scaled values from the Hartmann and Wenzel (1995) catalog. The Earth tide amplitudes show excellent agreement with the semi-diurnal tidal groups, but there is some additional noise that may be present at the diurnal frequencies possibly due to ocean loading, evapotranspiration, or other signals not considered in the model. Note the scale difference for the Earth tide and residuals.

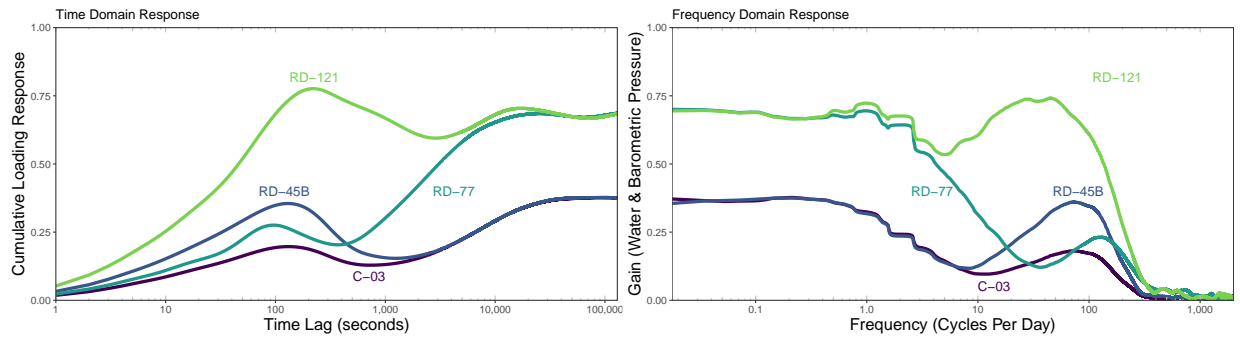


Figure 8: Comparison of well pairs (C-03 and RD-45B, RD-77 and RD-121). At early times each well has a unique response, but at late times the responses are indistinguishable for the well pairs.

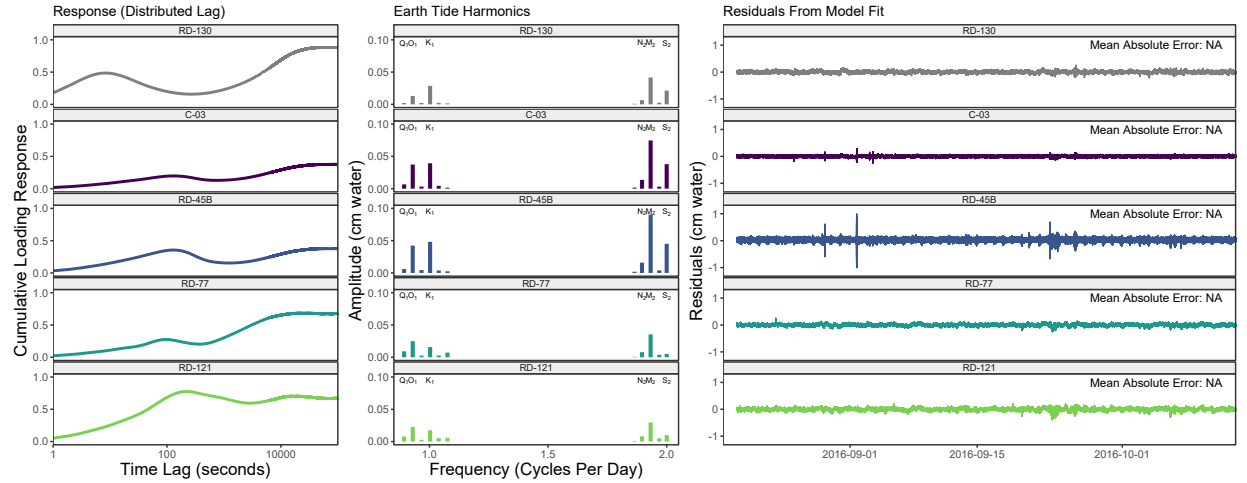


Figure 9: Summary of distributed lag model fits, Earth tide components and the residuals from the model fit. Given the proximity to the barometric pressure monitor, RD-130 provides the signal to noise ratio for the early time response. For RD-130, RD-77, and RD-121 which are considered unconfined, the Earth tide response is close to instrument precision and therefore increased uncertainty is associated with the values. C-03 and RD-45B are semi-confined and have Earth tide ratios between components that are consistent with theory providing increased confidence in the characterization. In general, the residuals are close to instrument precision with the largest residuals being associated with seismicity, which was not included in the regression model.

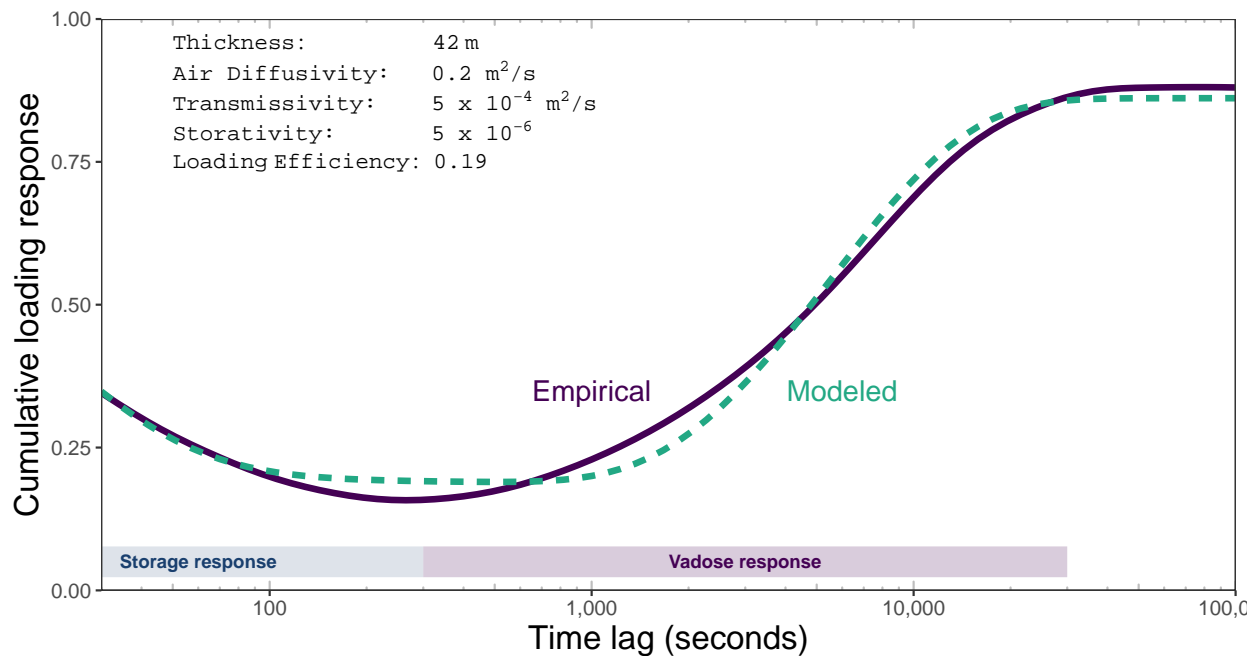


Figure 10: Response function determined with the distributed lag model and the combined well-bore storage and vadose air flow model fit. Parameters were fit using non-linear least squares with the Gauss-Newton algorithm. Some of the differences may be related to heterogeneity in the vadose zone resulting from faults and fractures.

678 **List of Tables**

679 1	Well construction details. Depth to water is the mean measurement for 2016-2019.	37
680 2	Estimates of loading efficiency using different static methods on noise free synthetic data. The expected value is presented in the column headings in parentheses. Clark's method was tested using two different sampling frequencies.	38
681 3	Efficiency and accuracy of the barometric response function methods. The distributed lag model tends to be more efficient in terms of computation time and memory usage. SE refers to the residual standard deviation between the predicted and known values, and CRF is the cumulative response function.	39
682		
683		
684		
685		
686		

Table 1: Well construction details. Depth to water is the mean measurement for 2016-2019.

Well	Diameter (m)	Interval top (mbgs)	Interval bottom (mbgs)	Top of casing (masl)	Depth to water (m)	Sat. interval (m)
C-03	0.1	6.1	138.7	561.1	66	72
RD-121	0.1	18.3	76.2	597.5	48	28
RD-130	0.11	12.2	53.3	573.5	42	12
RD-45B	0.17	164	179.8	560.9	66	16
RD-77	0.12	14	51.8	584.8	35	17

Table 2: Estimates of loading efficiency using different static methods on noise free synthetic data. The expected value is presented in the column headings in parentheses. Clark's method was tested using two different sampling frequencies.

Method	Confined (0.38)	Storage (0.0)	Vadose (1.0)	Combined (1.0)
Simplified Acworth	0.38	0.01	0.55	0.54
Least Squares	0.38	0.00	0.93	0.93
Clark (1 hr)	0.38	0.01	0.23	0.24
Clark (1 day)	0.38	0.00	0.94	0.94

Table 3: Efficiency and accuracy of the barometric response function methods. The distributed lag model tends to be more efficient in terms of computation time and memory usage. SE refers to the residual standard deviation between the predicted and known values, and CRF is the cumulative response function.

Δt	N terms	N obs.	Time	Memory	SE (cm)	Residuals 10^{-8} to 10^{-2}	CRF True Fit
<i>Regular lags</i>							
3600s	25	37	6.5ms	827KB	2.4×10^{-1}		
600s	145	217	22ms	3MB	1.9×10^{-1}		
15s	5761	8641	1.63m	4GB	4.7×10^{-2}		
<i>Irregular lags</i>							
1s	20	129604	140ms	198MB	2.8×10^{-1}		
1s	100	129604	1.1s	883MB	5.8×10^{-2}		
1s	400	129604	13s	3GB	1.8×10^{-2}		
<i>Distributed lags</i>							
1s	15	129604	230ms	167MB	1.1×10^{-1}		
1s	20	129604	270ms	213MB	1.6×10^{-2}		
1s	25	129604	380ms	259MB	2.4×10^{-3}		